Reactive High-Power Impulse Magnetron Sputtering of Chromium-Carbon Films

Chin-Chiuan Kuo [1,*], Chun-Hui Lin [1], Jing-Tang Chang [2] and Yu-Tse Lin [2]

[1] Department of Mechanical and Computer Aided Engineering, National Formosa University, Huwei, Yunlin County 63201, Taiwan; 10920110@gm.nfu.edu.tw

[2] Coating Department, Supati Corporation, Citong, Yunlin County 64747, Taiwan; jingtangc@gmail.com (J.-T.C.); d0875102@gm.nfu.edu.tw (Y.-T.L.)

* Correspondence: cckuo@nfu.edu.tw; Tel.: +886-5631-3492

check for updates

Abstract: Chromium-carbon films were deposited by utilizing reactive high-power impulse magnetron sputtering at different mixture ratios of ethyne and argon atmosphere, and different substrate bias voltages and deposition temperature, with the same pulse frequency, duty cycle, and average power. The microstructure and mechanical properties of the obtained films were compared. The films consist of amorphous or nanocrystalline chromium carbide, hydrogenated amorphous carbon, and minor α-chromium phase. Decreasing the fraction of ethyne increases the content of the α-chromium phase but decreases hydrogenated amorphous carbon phase. The film's hardness increases by enhancing the negative substrate bias and raising the deposition temperature, which could be attributed to the increase of film density and the Hall–Petch strengthening effect induced by the nanoscale crystallization of the amorphous carbide phase.

1. Introduction

The combination of chromium and carbon can synthesize various compounds, including metallic alloy, chromium carbides of different stoichiometric compositions, and carbon-based materials, which show different hardness, toughness, chemical stability, electrical conductivity, and tribological properties [1–8]. Metal-carbon thin films are easily synthesized via plasma-enhanced physical vapor depositions, such as cathodic arc ion plating [5,6,9], magnetron sputtering [10–15], electron-beam deposition [16,17], high-power impulse magnetron sputtering [12,18–20], and a hybrid method [21]. The hardness of chromium carbide is varied up to ten times depending on the deposition processes [13–15]. Therefore, carbide coatings are commonly used as an adhesion enhancement interlayer between metallic workpieces and an amorphous carbon topcoat [21,22]. The mechanisms of hardness enhancement for these carbides and carbon-based coatings are due to their nanocomposite structure. These coatings typically consist of an amorphous carbon (hydrogenated diamond-like or graphite-like a-C:H phase) and a crystalline metal or hard metal carbide phase [15,23]. The fractions of $sp3/sp2$ bonding ratio and nanocrystalline carbide phases influence the hardness, elastic modulus, and thermal stability of coatings [15,24]. The ratio of a-C:H and carbide phases is usually dominated by the mixture ratio of hydrocarbon and inert gas during the deposition [5–22], and the $sp3/sp2$ bonding ratio of a-C:H phases and grain size of carbides are strongly affected by the substrate bias voltage and the pulse width [6,14,18,19].

High-power impulse magnetron sputtering (HiPIMS) provides high power densities in pulses with a low duty cycle [25,26] on a magnetron sputtering source cathode, which enables high-density plasma

waves and fluxes of ionized sputtered source materials. This benefits the alteration of the kinetic energy of incident ions and the migration of adatoms through controlling substrate biasing and the pulse power density, which results in the variety of the microstructure, hardness, and adhesion of the obtained coatings [27–31]. However, the reactive HiPIMS deposition is much more complex [26]. Preventing the target poisoning and the consequent arc discharge on the source target restricts the region of the applied pulse width on the source target. Furthermore, applying a direct current high substrate bias voltage may result in the charging and arcing on a non-conductive compound coating [26,32], which also limits the region of substrate biasing. A pulsed substrate bias can effectively prevent this disadvantage [32], and increases the film density in the HiPIMS process [26,33]. Although the reactive sputter deposition of Cr–C films has been widely researched, the applications of the reactive HiPIMS deposition of such materials are still rare [20], and the usage of synchronized pulsed substrate bias is not reported in these articles. In this work, various Cr–C films were prepared using the HiPIMS technique, by introducing different mixture ratios of argon and ethyne and applying different synchronized pulsed substrate biases and different deposition temperatures for comparison.

2. Materials and Methods

The Cr–C films were deposited in a vacuum chamber with one unipolar HiPIMS power and one unipolar substrate bias power. The details of the power supplies, the target, the size of substrate samples, and the cleaning of substrate samples can be found in our previous work of chromium film [31]. Three different substrate materials had been polished and were simultaneously used, including an AISI M35 high-speed steel disc with a size of ϕ 30 × 1 (*h*) mm^2, a SUS 304 stainless steel mirror plate, and silicon wafer chips. After placing samples into the deposition chamber, vacuuming, and cleaning with argon plasma, the substrate temperature raised to about 190 °C without using additional substrate heating. For a higher deposition temperature, of 300 °C, the additional substrate heating would be applied during the argon plasma cleaning. The deposition parameters for Cr–C films are shown in Table 1.

Table 1. Parameters for the deposition of chromium-carbon films.

Deposition Parameters		Value
Atmosphere	Pressure (Pa)	0.8
	Ar/C$_2$H$_2$ flow ratio	1:1, 6:1, 8:1, 12:1
Target HiPIMS power	Average power (kW)	3
	Peak voltage (V)	−518~−612
	Peak current (A)	254~199
	Pulse frequency (Hz)	332
	Pulse width (μs)	60 (duty cycle 2%)
Cr ion bombardment	Synchronized bias voltage pulse	−1000 V (pulse width 96 μs)
	Bombardment time	40 s
Cr–C film deposition	Synchronized bias voltage pulse	Ground 0 V, −60 V, −150 V (pulse width 96 μs)
	Deposition time	10 min, 190 min
Deposition temperature (°C)		200, 300

Notes: high-power impulse magnetron sputtering (HiPIMS).

Different mixture ratios of argon/ethyne—1:1, 6:1, 8:1, 12:1—were respectively introduced to keep a deposition pressure 0.8 Pa for Cr–C film depositions. The applied target HiPIMS voltage pulses were near to a rectangle shape with a width of 60 μs and a frequency of 332 Hz. The pulse voltage and corresponding peak current on the target floated between −518 to −612 V due to the varying target conditions and the set deposition atmosphere. The pulse frequencies were manually set with the same pulse duty cycle, 2.5%, to maintain a constant target average power at 3 kW for all depositions.

As reported in the previous work [31], applying a pulsed substrate bias synchronized with the HiPIMS discharge pulse is helpful to selectively attract ions and the charged species with a stable bias

voltage and enable the target ion bombardment for a stronger film adhesion. The Cr ion bombardment was carried out before the Cr–C layer deposition. As the target HiPIMS pulse began, the substrate bias voltage pulse of −1000 V with a 1.75-fold pulse width of HiPIMS pulses was simultaneously initiated in order to accelerate Cr ions to bombard on the substrate. To minimize the roughness and temperature change on the substrate surface, the Cr ion bombardment was restricted to 40 s. After the bombardment, the substrate bias voltage switched to 0 V (grounded), pulsed −60 V, or pulsed −150 V directly without any gradient substrate biasing, to deposit different Cr–C films.

The microstructures of deposited films are observed by using a scanning electron microscope (SEM, S-4800 Cold Field Emission Scanning Electron Microscope, Hitachi, Tokyo, Japan). The film's thickness was estimated from cross-sectional SEM micrographs, and the crystallinity was characterized by utilizing an X-ray diffractometer (D8 Discover X-ray diffractometer, Bruker, Billerica, MA, USA). A Raman spectrometer (PROTRUSTECH, Tainan, Taiwan) was used to determine the presence of oxide and carbon phases in the Cr–C films. The nanoindentations (A TTX-NH3 nanoindentation tester, Anton Paar, Graz, Austria) were carried out to evaluate the film's hardness. Settings of analysis instruments were as the same as described in the references [30,31].

3. Results and Discussion

3.1. The Influences of Different Ar/C$_2$H$_2$ Flow Ratios

The Raman spectra of the Cr–C films deposited at different Ar/C$_2$H$_2$ flow ratios and the pressure of 0.8 Pa for 10 min are shown in Figure 1. Only two major peaks, the G (~1580 cm^{-1}) and D (~1350 cm^{-1}) bands of carbon phases, and a minor peak of Cr$_2$O$_3$ (~541 cm^{-1}) phase can be identified. The peaks of chromium carbides are very weak. This indicates that the microstructure of deposited Cr–C films could be a composite of amorphous carbide, amorphous carbon phases, and metallic chromium phases. The intensities of D and G decrease with the fraction of C$_2$H$_2$. However, the estimated I_D/I_G values of four samples are close to each other, with a difference of less than 2%, which means that the ratios of *sp*3 and *sp*2 bonds of the amorphous carbon phase of the four samples could be approximate. These results imply that the content of amorphous carbon phase decreases with the fraction of C$_2$H$_2$. A similar trend was also found in the direct current magnetron sputtering deposited Cr–C films [24].
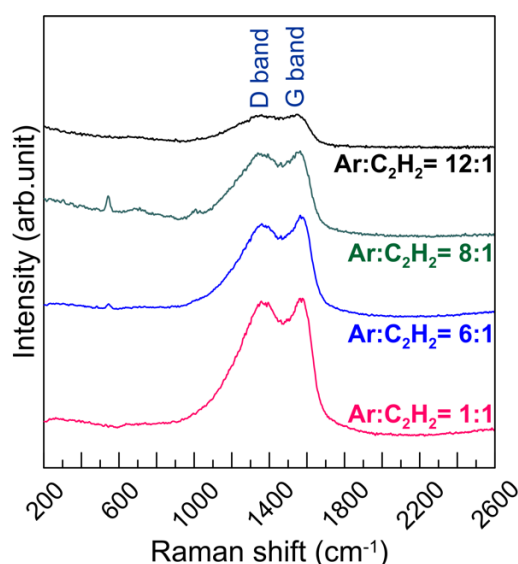

Figure 1. Raman spectra of Cr–C films deposited on the AISI M35 high-speed steel with a substrate bias of −60 V at a different Ar/C$_2$H$_2$ mixture atmosphere, of 0.8 Pa, for 10 min.

The X-ray diffractograms of the Cr-C films deposited at different Ar/C$_2$H$_2$ flow ratios are shown in Figure 2. There is no obvious diffraction peak in the diffractograms of films of Ar/C$_2$H$_2$ flow ratios of

1:1 and 6:1, which indicates that films deposited in this range of mixture ratio are amorphous or partial nanocrystalline. Weak peaks of α-chromium and chromium carbide phases appeared in the films of 8:1, and the peak intensity of the α-chromium phase became stronger in the film of 12:1. This indicates that the fraction of C_2H_2 may not be sufficient to react with the chromium species ejected from the target when the Ar/C_2H_2 flow ratio is higher than 8:1. The XRD results confirm the previous surmise about amorphous carbon and partly nanocrystalline carbide phases, which are similar to the reported Cr–C films by using sputtering [10,24,34]. The intensity around 40° slightly increases with decreasing C_2H_2. This trend is also similar to the dc magnetron sputtering deposited Cr–C films [24].
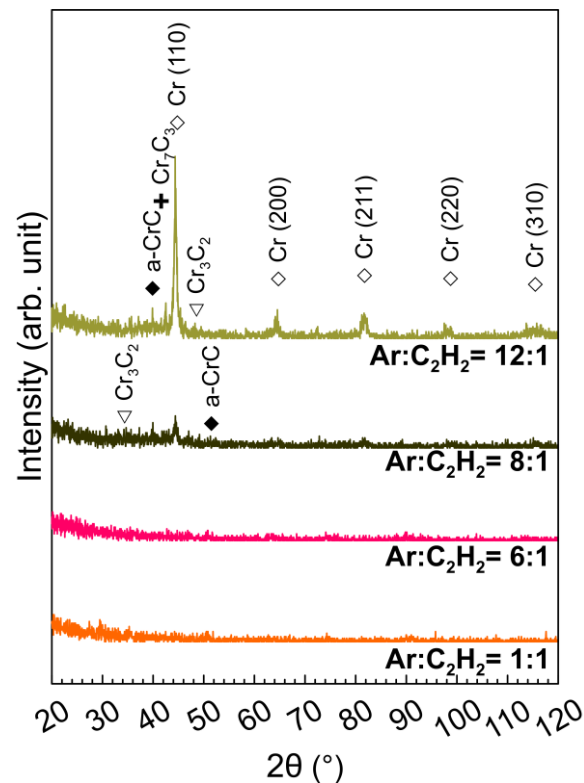

Figure 2. X-ray diffractograms of Cr–C films deposited on the AISI M35 high-speed steel with a substrate bias of −60 V at different Ar/C_2H_2 mixture ratio atmosphere, of 0.8 Pa, for 10 min.

The top and cross-sectional SEM SE images of the Cr–C films deposited at the pressure of 0.8 Pa with different Ar/C_2H_2 flow ratios are shown in Figure 3. The film of 1:1 presents a loosen structure of stacking clusters, which is similar to the reported sputtering-deposited Cr–C films with a high carbon content [10]. By increasing the fraction of argon, the film structure becomes denser and more columnar, without any granular edge, which is similar to the reported sputtering and HiPIMS-deposited Cr-C films with lower carbon contents [10,12]. These features of amorphous film are consistent with the results of XRD. The estimated deposition rates for Ar/C_2H_2 ratios of 1:1, 6:1, 8:1, and 12:1 are 70, 153, 100, and 122 nm/min, respectively. The partial pressure of argon with an Ar/C_2H_2 ratio of 1:1 might be too low to sputter chromium atoms efficiently. On the other hand, the films of 1:1 and 6:1 were too fragile for hardness and adhesion tests. For these reasons, only the ratio of 8:1 were used in the following experiments of different substrate bias voltage and deposition temperature. The deposition time was also extended to 190 min.
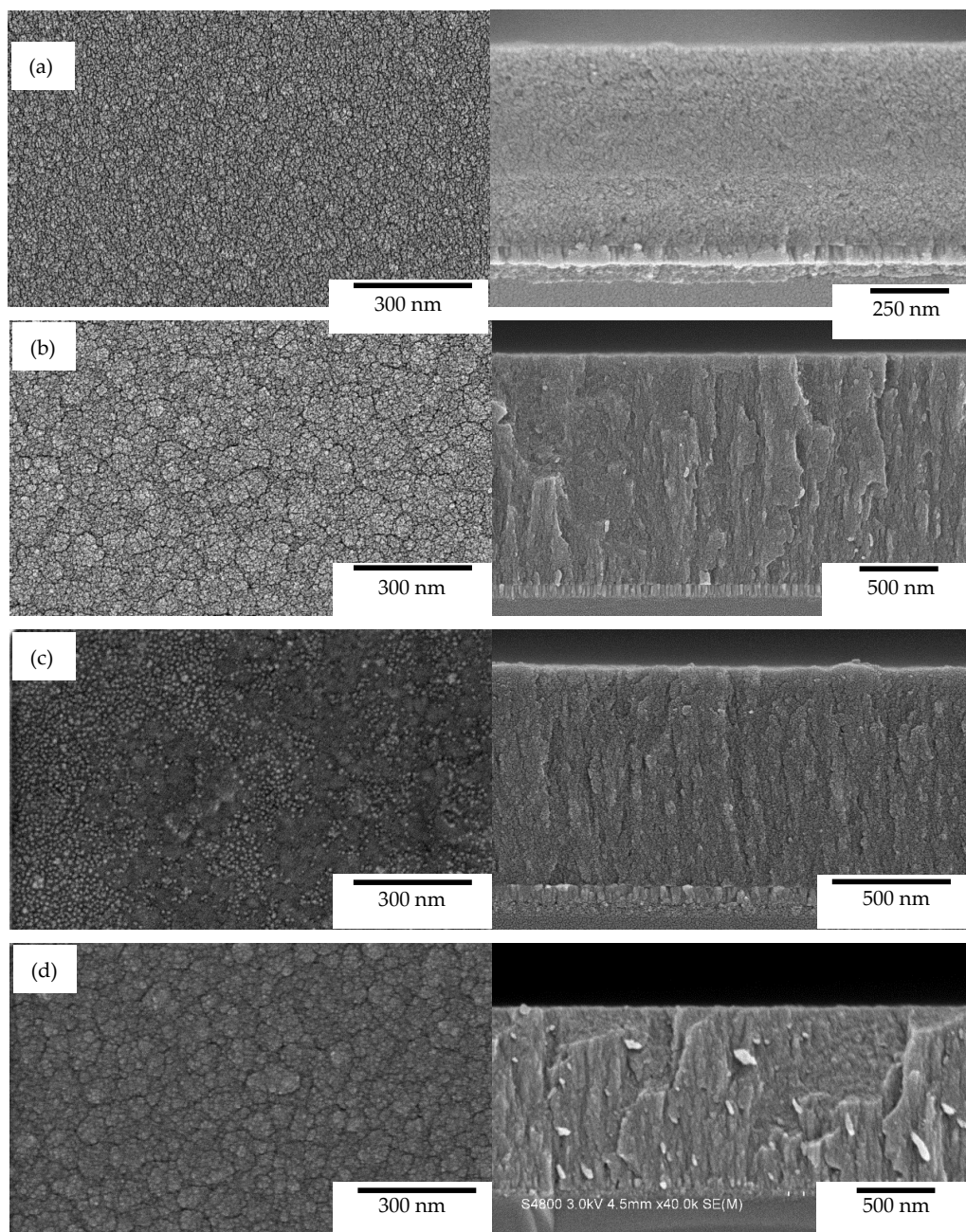
Figure 3. Top (left side) and cross-sectional (right side) SEM SE micrographs of Cr–C films deposited at the deposition pressure of 0.8 Pa with the Ar/C$_2$H$_2$ mixture ratio of (**a**) 1:1, (**b**) 6:1, (**c**) 8:1, and (**d**) 12:1 on a silicon wafer chip (substrate bias −60 V) for 10 min.

3.2. Influences of the Synchronized Substrate Bias and Deposition Temperature

The X-ray diffractograms of the Cr–C films deposited at the pressure 0.8 Pa with the same Ar/C$_2$H$_2$ flow ratio, 8:1, but different substrate bias voltages are shown in Figure 4. All samples of the different substrate bias voltages are amorphous with minor α-chromium phases. The intensity around 40° is relatively stronger in films deposited with negative biases. A similar phenomenon was also found in Cr–C films prepared by using vacuum arc [6,22], sputtering [12,23], and HiPIMS [12,18] depositions in an Ar/carbon hydride atmosphere. This suggests the formation of some nanocrystalline CrC with applying negative substrate bias due to the kinetic energy enhancement of incident ions [27–29]. A contrary phenomenon in Figure 4, which has never been reported in other similar researches, is that

the intensity of the α-chromium phase decreases by enhancing the substrate bias. Since the relative intensity of α (200) does not change, it is unlike the preferred orientation change resulting from the substrate biasing [31]. Besides, the −60 V substrate bias is not strong enough to cause an obvious re-sputtering of light elements [22]. One possible reason is that the negative substrate bias promotes the formation of carbide phases [22], and therefore reduces the fraction of α-chromium phases.
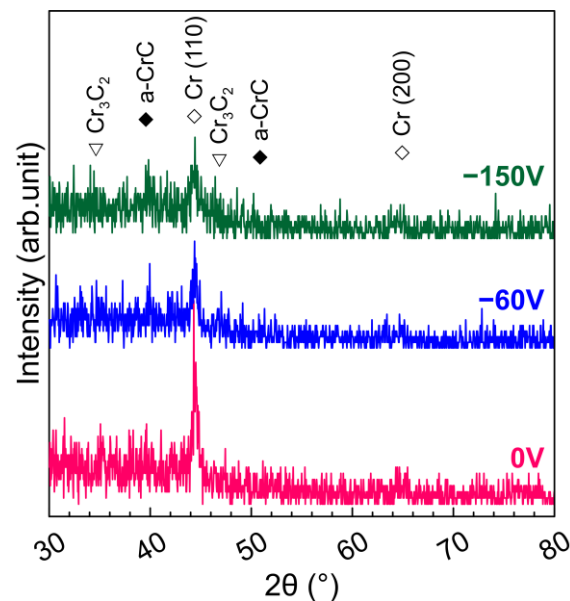

Figure 4. X-ray diffractograms of Cr-C films deposited on the AISI M35 high-speed steel with different substrate bias voltages at the same atmosphere of 0.8 Pa and Ar/C_2H_2 flow ratio of 8:1 for 190 min.

The cross-sectional SEM SE images of the Cr–C films deposited at the pressure of 0.8 Pa and the Ar/C_2H_2 flow ratio 8:1 but with different synchronized substrate bias voltages are shown in Figure 5. The film becomes more solid, and the fracture surface becomes smoother and more brittle, with enhancing the negative substrate bias. This also evidences the increase of kinetic energy incident ions and adatoms to form a denser structure. The nanoindentation results of the Cr–C film deposited with different substrate bias voltages shown in Figure 6 indirectly proves the densified film structure. The hardness of films increases by enhancing the negative substrate bias, which is similar to the results of vacuum arc deposited and the HiPIMS-deposited Cr–C films [6,12].
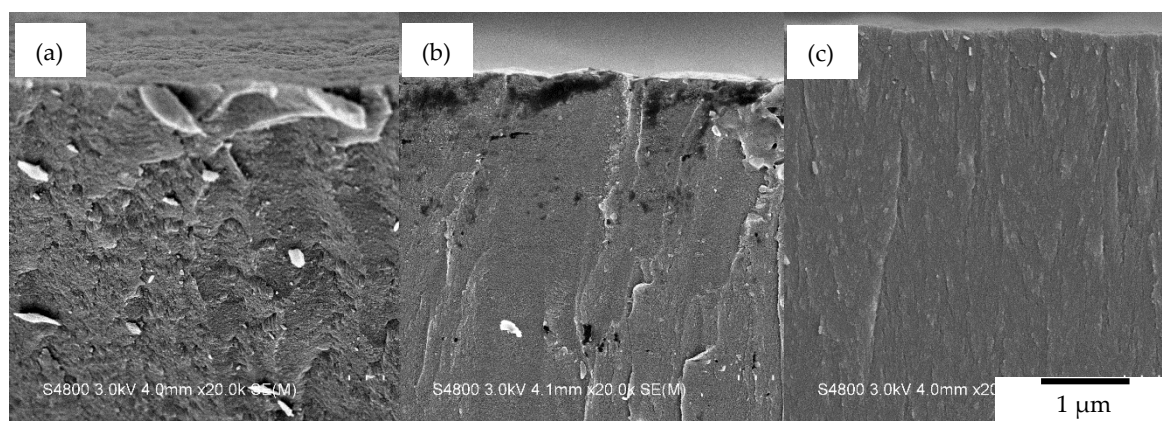

Figure 5. Cross-sectional SEM SE micrographs of Cr films deposited on a silicon wafer chip with the synchronized substrate bias voltage of (**a**) 0 V, (**b**) −60 V, and (**c**) −150 V, at the deposition pressure of 0.8 Pa with an Ar/C_2H_2 mixture ratio of 8:1 for 190 min.
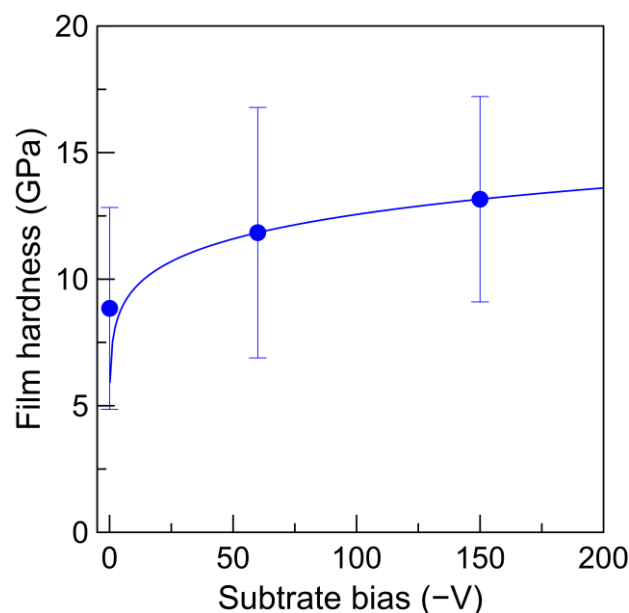
Figure 6. Film hardness versus the synchronized substrate bias voltage for Cr–C films deposited on the AISI M35 high-speed steel at a pressure of 0.8 Pa and the Ar/C$_2$H$_2$ mixture ratio of 8:1 for 190 min.

Since most of the obtained films in this work are thinner than 2 μm, the indentations were carried out with a max load of 5 mN and a 10-s pause to avoid the influences of substrate materials. The large measurement error could therefore be attributed to the microscale nonuniformity in the film structure. There are several phases, including a-Cr$_x$C$_y$, a-C:H, Cr, Cr$_3$C$_2$, and droplets. The domain size of different phases could vary from several nanometers to a micrometer [10,22,23]. The reported hardness value of HiPIMS-deposited a-C:H could be higher than 30 GPa, and the hardness value of HiPIMS-deposited Cr could be lower than 7 GPa [12,18–20,31]. Such great difference between different phases might be the reason of the high measurement error.

The Cr–C film deposited at 300 °C and the same substrate bias of −150 V in the same atmosphere present a cross-sectional microstructure similar to that of the film deposited at 200 °C. The hardness of the film deposited at 300 °C is 14.46 ± 5.24 GPa, which is about 10% higher than the one at 200 °C. The higher deposition temperature enables a higher mobility of adatoms, to form a denser and crystalline structure which usually results in more hardness. The X-ray diffractograms of the Cr–C films deposited at 200 °C and 300 °C are compared in Figure 7. Peaks of stoichiometric carbide phases slightly increase and peaks of amorphous carbide phase slightly weaken by raising the deposition temperature. This indicates that a higher temperature may promote the formation of stoichiometric carbide phases rather than an amorphous carbide phase. According to the Hall–Petch effect, the appearance of nanoscale grains may provide a grain boundary and strengthen the hardness of materials [18,35]. This could be one of the reasons for the higher hardness of Cr–C films deposited at 300 °C.

Deposition at a higher temperature is not recommended due to two reasons. One reason is that a higher temperature induces the conversion from hydrogenated amorphous carbon to nano-crystalline graphite [36], which usually results in the decrease of film hardness. Another reason depends on the heating method and consequent target conditions. The heating region should be restricted to the substrate. Heating the target surface should be avoided to minimize the target poisoning in such reactive sputtering [26]. In particular, the target for the HiPIMS process requires abundant cooling to release the heat generated by the high-density power input during the pulse on time. The carbides formed on the target surface due to poisoning are potential initiation points of the arc discharge and accompanying ejection of droplets during the high-power pulse on time. The droplets embedded in the Cr–C films with a size of several micrometers are detrimental to the film uniformity, density, adhesion, and consequent performances.
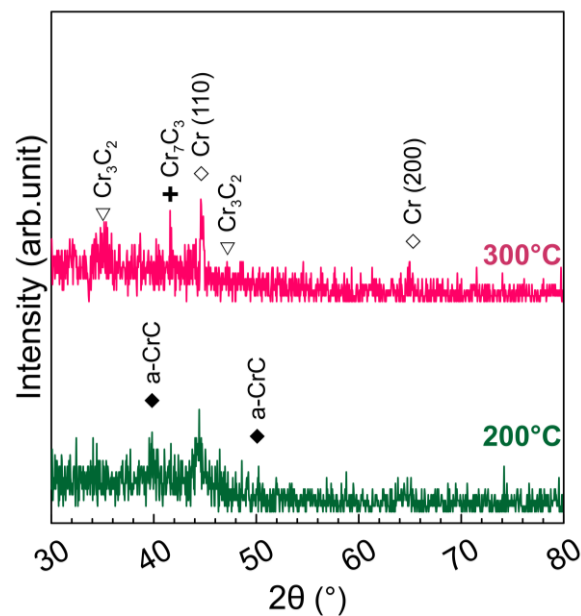
Figure 7. X-ray diffractograms of Cr-C films deposited on the AISI M35 high-speed steel at different deposition temperatures in the atmosphere of 0.8Pa and Ar/C_2H_2 mixture ratio of 8:1 with a substrate bias voltage of −150 V for 190 min.

The above results indicate that applying the reactive HiPIMS deposition to synthesized Cr–C films can lead to a film structure, composition, and hardness similar to the one obtained by using direct current magnetron sputtering. Although the disadvantages of reactive direct current magnetron sputtering, such as the target poisoning and hysteresis, also occur in the reactive HiPIMS deposition, these can nevertheless be reduced by controlling the HiPIMS pulse frequency and duty cycle [26]. The results in this work indicate that applying the synchronized substrate bias can easily alter the film structure and film density at a relatively lower substrate temperature, due to the high ionization ratio in HiPIMS deposition.

4. Conclusions

This research preliminarily investigates the influences of reactive gas C_2H_2 ratio, synchronized substrate bias voltage, and deposition temperature on the Cr–C films deposited by using reactive high-power impulse magnetron sputtering with the same average power, pulse frequency, and pulse duty cycle at a constant pressure of 0.8 Pa. All the Cr–C films obtained in this work are mainly amorphous. The films consists of amorphous or nanocrystalline chromium carbide, hydrogenated amorphous carbon, and a minor α-chromium phase. Increasing the Ar/C_2H_2 ratio increases the content of the α-chromium phase but decreases the hydrogenated amorphous carbon phase. Increasing the Ar/C_2H_2 ratio also promotes the film structure to change from loose stacking clusters into a solid columnar feature. Applying synchronized negative substrate bias also densifies the film structure and enhances the film hardness. Same enhancements can also be achieved by raising the substrate temperature, but not over 300 °C. The nanocrystallization of amorphous carbide phases promoted by negative substrate bias and substrate temperature induces the Hall–Petch strengthening effect and results in a higher film hardness.

Author Contributions: Conceptualization, C.-C.K.; data curation, C.-H.L.; investigation, J.-T.C., C.-H.L., and Y.-T.L.; methodology, C.-C.K. and C.-H.L.; project administration, C.-C.K.; supervision, C.-C.K.; visualization, J.-T.C. and C.-H.L.; writing–original draft, J.-T.C. and C.-C.K.; writing–review and editing, C.-C.K. All authors have read and agreed to the published version of the manuscript.

Conflicts of Interest: The authors declare no conflict of interest.

References

1. Komiya, S.; Ono, S.; Umezu, N.; Narusawa, T. Characterization of thick chromium-carbon and chromium-nitrogen films deposited by hollow cathode discharge. *Thin Solid Films* **1977**, *45*, 433–445. [CrossRef]

2. Toth, L.E. *Transition Metal Carbides and Nitrides*; Academic Press: New York, NY, USA, 1971; pp. 1–25.

3. Aubert, A.; Gillet, R.; Gaucher, A.; Terrat, J.P. Hard chrome coatings deposited by physical vapour deposition. *Thin Solid Films* **1983**, *108*, 165–172. [CrossRef]

4. Pierson, H.O. *Handbook of Refractory Carbides and Nitrides*, 1st ed.; Noyes Publications: New Jersey, NJ, USA, 1996; pp. 100–116.

5. Merl, D.K.; Panjan, P.; Čekada, M.; Maček, M. The corrosion behavior of Cr–(C,N) PVD hard coatings deposited on various substrates. *Electrochim. Acta* **2004**, *49*, 1527–1533. [CrossRef]

6. Lin, C.C.; Lee, J.W.; Chang, K.L.; Hsieh, W.J.; Wang, C.Y.; Chang, Y.A.; Shih, H.C. The effect of the substrate bias voltage on the mechanical and corrosion properties of chromium carbide thin films by filtered cathodic vacuum arc deposition. *Surf. Coat. Technol.* **2006**, *200*, 2679–2685. [CrossRef]

7. Edigaryan, A.A.; Safonov, V.A.; Lubnin, E.N.; Vykhodtseva, L.N.; Chusova, G.E.; Polukarov, Y.M. Properties and preparation of amorphous chromium carbide electroplates. *Electrochim. Acta* **2002**, *47*, 2775–2786. [CrossRef]

8. Chung, D.D.L. *Carbon Composites: Composites with Carbon Fibers, Nanofibers and Nanotubes*, 2nd ed.; Elsevier: Amsterdam, The Netherlands, 2017; pp. 387–466. [CrossRef]

9. Esteve, J.; Romero, J.; Go´mez, M.; Lousa, A. Cathodic chromium carbide coatings for molding die applications. *Surf. Coat. Technol.* **2004**, *188–189*, 506–510. [CrossRef]

10. Andersson, M.; Högström, J.; Urbonaite, S.; Furlan, A.; Nyholm, L.; Jansson, U. Deposition and characterization of magnetron sputtered amorphous Cr–C films. *Vacuum* **2012**, *86*, 1408–1416. [CrossRef]

11. Maréchal, N.; Quesnel, E.; Pauleau, Y. Deposition process and characterization of chromium-carbon coatings produced by direct sputtering of a magnetron chromium carbide target. *J. Mater. Res.* **1994**, *9*, 1820–1828. [CrossRef]

12. Nygren, K.; Samuelsson, M.; Flink, A.; Ljungcrantz, H.; Rudolphi, Å.K.; Jansson, U. Growth and characterization of chromium carbide films deposited by high rate reactive magnetron sputtering for electrical contact applications. *Surf. Coat. Technol.* **2014**, *260*, 326–334. [CrossRef]

13. Dai, W.; Wu, G.; Wang, A. Structure and elastic recovery of Cr-C:H films deposited by a reactive magnetron sputtering technique. *Appl. Surf. Sci.* **2010**, *257*, 244–248. [CrossRef]

14. Ziebert, C.; Ye, J.; Stüber, M.; Ulrich, S.; Edinger, M.; Barzen, I. Ion bombardment-induced nanocrystallization of magnetron-sputtered chromium carbide thin films. *Surf. Coat. Technol.* **2011**, *205*, 4844–4849. [CrossRef]

15. Gassner, G.; Mayrhofer, P.H.; Mitterer, C.; Kiefer, J. Structure-property relations in Cr-C/a-C:H coatings deposited by reactive magnetron sputtering. *Surf. Coat. Technol.* **2005**, *200*, 1147–1150. [CrossRef]

16. Poletika, I.M.; Ivanov, S.F.; Gnyusov, S.F.; Perovskaya, M.V. Electron-beam deposition of chromium carbide–based coatings with an ultradispersed structure or a nanostructure. *Russ. Metall.* **2016**, 1275–1282. [CrossRef]

17. Wolfe, D.E.; Singh, J.; Narasimhan, K. Synthesis of titanium carbide/chromium carbide multilayers by the co-evaporation of multiple ingots by electron beam physical vapor deposition. *Surf. Coat. Technol.* **2002**, *160*, 206–218. [CrossRef]

18. Li, Z.-L.; Chen, Y.-Y.; Wang, C.-J.; Lee, J.-W. Comparison of chromium carbide thin films grown by different power supply systems. *Surf. Coat. Technol.* **2018**, *353*, 329–338. [CrossRef]

19. Konishi, T.; Yukimura, K.; Takaki, K. Fabrication of diamond-like carbon films using short-pulse HiPIMS. *Surf. Coat. Technol.* **2016**, *286*, 239–245. [CrossRef]

20. Tillmann, W.; Dias, N.F.L.; Stangier, D. Tribo-mechanical properties of CrC/a-C thin films sequentially deposited by HiPIMS and mfMS. *Surf. Coat. Technol.* **2018**, *335*, 173–180. [CrossRef]

21. Richert, M.; Mazurkiewicz, A.; Smolik, J. Chromium carbide coatings obtained by the hybrid PVD methods. *J. Achiev. Mater. Manuf. Eng.* **2010**, *43*, 145–152.

22. Yate, L.; Martínez-de-Olcoz, L.; Esteve, J.; Lousa, A. Effect of the bias voltage on the structure of nc-CrC$_x$/a-C:H coatings with high carbon content. *Surf. Coat. Technol.* **2012**, *206*, 2877–2883. [CrossRef]

23. Singh, V.; Jiang, J.C.; Meletis, E.I. Cr-diamond like carbon nanocomposite films: Synthesis, characterization and properties. *Thin Solid Films* **2005**, *489*, 150–158. [CrossRef]

24. Gassner, G.; Patscheider, J.; Mayrhofer, P.H.; Mitterer, C. Thermal stability of nanocomposite CrC/a-C:H thin films. *Thin Solid Films* **2007**, *515*, 5411–5417. [CrossRef]

25. Lundin, D.; Minea, T.; Gudmundsson, J.T. *High Power Impulse Magnetron Sputtering: Fundamentals, Technologies, Challenges and Applications*; Elsevier: Amsterdam, The Netherlands, 2019; ISBN 9780128124543.

26. Anders, A. Tutorial: Reactive high power impulse magnetron sputtering (R-HiPIMS). *J. Appl. Phys.* **2017**, *121*, 171101. [CrossRef]

27. Anders, A.; Andersson, J.; Ehiasarian, A. High power impulse magnetron sputtering: Current-voltage-time characteristics indicate the onset of sustained self-sputtering. *J. Appl. Phys.* **2007**, *102*, 113303. [CrossRef]

28. Kouznetsov, V.; Macak, K.; Schneider, J.; Helmersson, U.; Petrov, I. Hybrid HIPIMS and DC magnetron sputtering deposition of TiN coatings: Deposition rate, structure and tribological properties. *Surf. Coat. Technol.* **1999**, *12*, 290. [CrossRef]

29. Machunze, R.; Ehiasarian, A.; Tichelaar, F.; Janssen, G.; Ehiasarian, A. Stress and texture in HIPIMS TiN thin films. *Thin Solid Films* **2009**, *518*, 1561–1565. [CrossRef]

30. Kuo, C.C.; Lin, Y.T.; Chan, A.; Chang, J.T. High temperature wear behavior of titanium nitride coating deposited using high power impulse magnetron sputtering. *Coatings* **2019**, *9*, 555. [CrossRef]

31. Kuo, C.C.; Lin, C.H.; Lin, Y.T.; Chang, J.T. Effects of cathode voltage pulse width in high power impulse magnetron sputtering on the deposited chromium thin films. *Coatings* **2020**, *10*, 542. [CrossRef]

32. Greczynski, G.; Lu, J.; Jensen, J. Metal versus rare-gas ion irradiation during Ti$_{1-x}$Al$_x$N film growth by hybrid high power pulsed magnetron/dc magnetron co-sputtering using synchronized pulsed substrate bias. *J. Vac. Sci. Technol.* **2012**, *30*, 061504. [CrossRef]

33. Cooke, K.E.; Hampshire, J.; Southall, W.; Teer, D.G. Industrial application of pulsed dc bias power supplies in closed field unbalanced magnetron sputter ion plating. *Surf. Eng.* **2004**, *20*, 189–195. [CrossRef]

34. Jellad, A.; Labdi, S.; Malibert, C.; Renou, G. Nanomechanical and nanowear properties of Cr$_3$C$_2$ thin films deposited by rf sputtering. *Wear* **2008**, *264*, 893–898. [CrossRef]

35. Guisbiers, G.; Herth, E.; Buchaillot, L.; Pardoen, T. Fracture toughness, hardness, and Young's modulus of tantalum nanocrystalline films. *Appl. Phys. Lett.* **2010**, *97*, 143115. [CrossRef]

36. Tallant, D.R.; Parmeter, J.E.; Siegal, M.P.; Simpson, R.L. The thermal stability of diamond-like carbon. *Diam. Relat. Mater.* **1995**, *4*, 191–199. [CrossRef]